DOI: 10.3969/j.issn.1673-3185.2017.06.011 **http**: // english.ship-research.com

Translated from: ZHENG H W, CHEN C H, HOU H L, et al. Simulation analysis of effects of single fragment size on air-blast wave and fragment propagation[J]. Chinese Journal of Ship Research, 2017, 12(6): 73-80.

Simulation analysis of effects of single fragment size on air-blast wave and fragment propagation

ZHENG Hongwei, CHEN Changhai, HOU Hailiang, ZHU Xi, LI Dian

Department of Naval Architecture Engineering, Naval University of Engineering, Wuhan 430033, Hubei, China

Abstract: [Objectives] This paper involves the propagation and attenuation of the velocity and energy of air-blast waves and high-velocity fragments while taking their combined effects into account. **[Methods]** With ANSYS/LS-DYNA software, a simulation model of a columnar TNT air-blast is built with prefabricated fragments affixed to its end. When the total quality of fragments is constant, the effects of a single fragment's size on the propagation of the air-blast wave and fragments are studied by changing the size of the single fragment. **[Results]** The results show that fragments greatly reduce the intensity and velocity of a shockwave, and block the air-blast waves behind them. When the total quality of the fragments remains constant, the effects of single fragment size on blast shock wave propagation characteristics show little difference. The smaller the single fragment, the more kinetic energy the fragments will have and the faster that energy will dissipate. **[Conclusions]** As a result, more attention should be paid to the combined effects of air-blast waves and high-velocity fragments. Such research can provide reference points for the deeper study of blast loads and their interaction.

Key words: explosion mechanics; air-blast wave; high-velocity fragment; numerical simulation; fragment size

CLC number: U661.43; O383$^+$.3

0 Introduction

With the rapid development of modern weapons, anti-ship missiles have become one of the hotspots in the research of weapons today. The shock waves and a large number of high-velocity fragments caused by missile explosion are two major destructive elements acting on structure in a combined way [1-2]. In the forming stage of blast loads, shell broke into fragments, and the air around the shell formed a shock wave under the action of detonation. The material properties, thickness, charge amount, type of charge, shell shape and initiation way of warhead shell all had a certain effect on the formation of shock wave and high-velocity fragments[3-5]. In 2014, Kong et al.[6] studied the spatial distribution and velocity property of the natural fragments caused by warhead shell by using numerical simulation, and pointed out that the maximum fragment velocity is at end cap, and fragment length was mainly determined by the difference of axial expansion strain rate of cylindrical shell. At this stage, the interaction between shock wave and fragment mainly showed that the energy generated by the explosion was partially dissipated to the formation of fragments, thus reducing the energy of shock wave[7]. Shock wave was a strong accelerating factor for fragments[8]. After the fragments were accelerated, they would obtain a high instantaneous initial velocity. The initial velocity of the fragment can be described by Gurney's formula[9]. Feng et al. [10], Zhang et al. [11] and Chen et al.[12] conducted a lot of studies on the initial velocity of fragments, and modified Gurney's formula successively by considering the rarefaction wave of detonation product, charge density changes, fragment size, fragment gap and other factors in combination with tests.

Received: 2017-04-13

Supported by: National Key Basic Research Project; National Natural Science Foundation of China (51409253, 51679246)

Author(s): ZHENG Hongwei, male, born in 1992, master candidate. Research interest: ship structure strength. E-mail: zhw_hit@163.com

CHEN Changhai (Corresponding author), male, born in 1985, Ph.D., lecturer, Research interests: anti-explosion and anti-impact of ship structure. E-mail: chenchanghai0746@163.com

When there was a balance between the resistance on fragments and thrust by detonation products, fragment velocity reached its maximum. Afterwards, the attenuation of the flying velocity of fragments would be closely related to fragment mass, windward area and other factors [13-14]. For the intensity and attenuation of air-blast shock wave, there had been a large number of experimental and empirical formula studies in China and abroad. Gong et al.[15] deduced the whole solving process of the encountering of fragment and shock wave by using Visual C++ theory. Gong pointed out that there were mainly three stages during the encountering of fragment and shock wave, including shock waves in the front, fragments and shock waves encountering and fragments exceeding shock waves and propagating in the front. The increases of explosive filling coefficient, detonation heat and velocity, fragment mass would reduce the distance from the explosion center to the encountering location to a certain extent[16].

For the formation of shock waves and high-velocity fragments, and the attenuation and encountering between the two, a large number of studies had been carried out in China and abroad. However, for the studies of shock wave and high-velocity fragment, most of them still decoupled the two kinds of loads and considered the combined loads as two kinds of loads for separate studies. Considering that there were fewer studies on the propagation process of the interaction between air-blast shock wave and high-velocity fragments, and there were some differences in the role of fragments with different sizes in this process, the propagation of the interaction between fragment and shock wave was a very complex physical and mechanical process, so it was difficult to analyze and study it by the theoretical method. Therefore, numerical simulation method would be used in this paper to establish finite element analysis model and investigate the influence law of fragment size on shock wave and fragment propagation.

1 Model establishment and verification of simulation method

1.1 Influence of mesh size on calculation results

In this paper, ANSYS/LS-DYNA nonlinear dynamic finite element analysis program is adopted for simulation calculation. An explosion model of square explosive with a side length of 50 mm in air region is established, and the ratio of side length of the square explosive to mesh size is defined as mesh density. The simulation models with mesh density of 2, 4, 6, 8, 10 and 20 are calculated, and the 1/8 model is shown in Fig. 1.

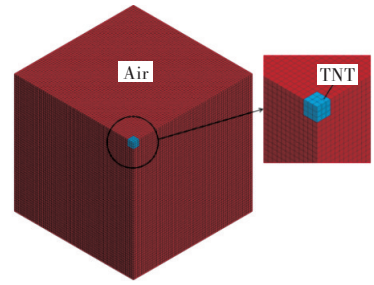

Fig.1 The six-meshes density model

Fig. 2 shows the overpressure time-history curve at 0.25 m in the case of different mesh densities, and Fig. 3 shows the curve of peak pressure ΔP_m at 0.25 and 0.40 m as the function of mesh density. As can be seen from Fig. 2 and Fig. 3, with the increase of mesh density, the calculated time of shock wave pressure climbing to peak overpressure decreases, and the peak pressure increases. While there is a significant peak clipping phenomenon in the calculated results under low mesh density, so the calculated results are smaller. When mesh density increases over 10, the effect of mesh size on the calculated results decreases. It can be considered that the denser the

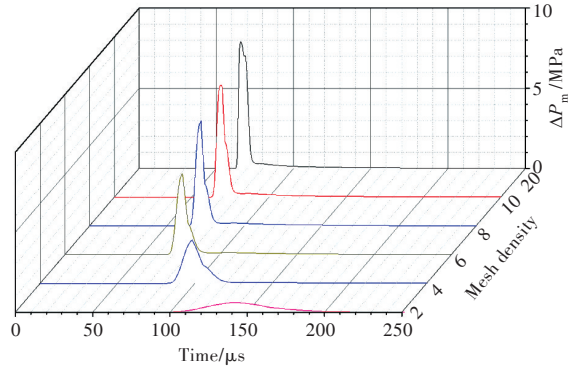

Fig.2 Peak overpressure of blast wave at 0.25 m

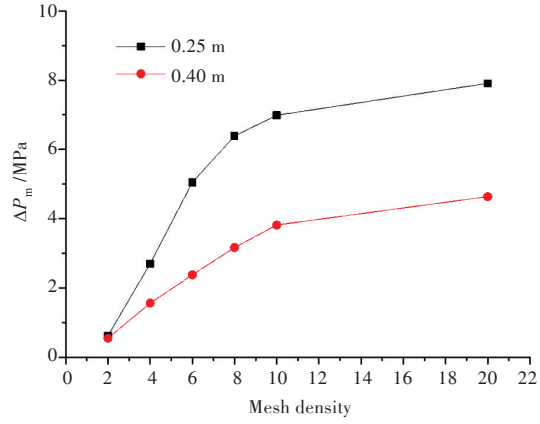

Fig.3 Peak overpressure of different mesh density at 0.25 and 0.40 m

mesh is, the closer the calculated results are to the true values is as long as some conditions are fulfilled.

1.2 Establishment of model

The model consists of three parts, including air region, fragments, and explosives. The filling of cylindrical explosives is completed by setting keywords of *INITIAL_VOLME_FRACTION_GEOMETRY. Taking into account the influence of mesh size and method of explosive filling, the mesh density of model should be as high as possible. However, in finite element analysis, the more detailed the unit division is, the more the number of nodes is; the shorter the calculation step is; and the longer the calculation time is. In order to reduce the calculation time, and taking into account the symmetry of air, explosives and fragments, the model uses two rounds of cylindrical casting TNT explosives, and adopts overlay arrangement and central explosion method. The 1/8 model is built, and symmetrical boundary conditions are set on the symmetry plane of model, while non-response boundary conditions are set on the rest planes. The calculation step coefficient is selected as 0.65. The size of air region is selected as 500 mm × 500 mm × 1 500 mm, and the schematic diagram of model layout and model size section are shown in Fig. 4. Mesh refinement is conducted on the square air region with the side length of 200 mm near explosives. After the refinement, the side length of hexahedral meshes is about 4 mm, and axial direction adopts gradient meshes. Finally, the total number of air region units obtained by division is about 144×10^4. The Euler unit is used for both explosives and air regions, and multi-material unit ALE algorithm is applied. Moreover, Lagrange unit is adopted for prefabricated fragments. The coupled algorithm between fragments and air materials is defined through the keywords of *CON-STRAINED_LAGRANGE_IN_SOLID.

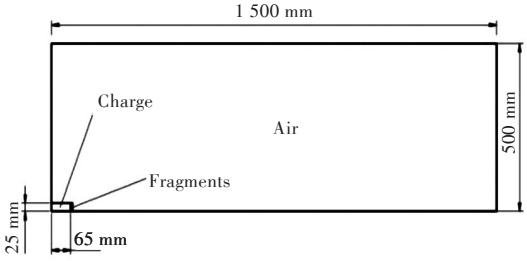

Fig.4 Schematic diagram of the model (1/8)

The explosives adopt *MAT_HIGH_EXPLOSIVE_BURN constitutive model and the expansion of detonation products are described by *EOS_JWL state equation:

$$P = A\left(1 - \frac{\omega}{R_1 V}\right)e^{-R_1 V} + B\left(1 - \frac{\omega}{R_2 V}\right)e^{-R_2 V} + \frac{\omega e_0}{V} \quad (1)$$

where P is detonation pressure; e_0 is the internal energy of initial explosive per unit volume; V is relative volume; e is exponential function; A, B, R_1, R_2 and ω are constants defined in the test, which are affected by factors such as charge density and explosive type. The detailed parameters are shown in Table 1 [17]. In the table, ρ is charge density; D is detonation velocity; P_{cj} is the pressure of detonation wave front; and V_0 is the initial relative volume. The firing time of each explosive unit is determined by the distance from this unit to the detonation point and the detonation velocity.

Table 1 The parameters of TNT materials and Equation of State(EOS)

Parameter	Numerical value	Parameter	Numerical value
A/GPa	309	V_0	1
B/GPa	3.90	e_0/(GJ·m^{-3})	6.2
R_1	4.485	ρ/(kg·m^{-3})	1 590
R_2	0.79	D/(m·s^{-1})	6 880
ω	0.30	P_{cj}/GPa	19.4

*MAT_NULL material model and *EOS_LINEAR_POLYNOMIAL state equation are used to describe air. The linear polynomial of state equation is:

$$P = C_0 + C_1\mu + C_2\mu^2 + C_3\mu^3 + (C_4 + C_5\mu + C_6\mu^2)e_0 \quad (2)$$

where $\mu = 1/V - 1$, $C_0 - C_6$ are polynomial coefficients. When the linear polynomial equation of state is used for ideal gas model, the material parameters of air and state equation are shown in Table 2.

Table 2 The parameters of air materials and EOS

Parameter	Numerical value	Parameter	Numerical value
C_0/MPa	−0.1	C_5	0.4
C_1	0	C_6	0
C_2	0	V	1
C_3	0	e_0/MPa	0.25
C_4	0.4	ρ/(kg·m^{-3})	1.25

Fragments use bilinear elasto-plastic constitutive model *MAT_PLASTIC_KINEMATIC, whose strain rate is defined by Cowper-Symonds model. The strain equation is:

$$\sigma_d = \left(\sigma_0 + \frac{EE_h}{E - E_h}\varepsilon_p\right)\left[1 + \left(\frac{\dot{\varepsilon}}{G}\right)^{1/n}\right] \quad (3)$$

where σ_d is dynamic yield strength; σ_0 is static yield strength; E is elastic modulus, and $E = 2.10 \times 10^5$GPa;

E_h is the hardening modulus; ε_p is effective plastic strain. $\dot{\varepsilon}$ is equivalent plastic strain rate; G and n are constants. For common soft steel, usually G = 40.4 s^{-1}, and n = 5 [18–22]. Fragment density ρ = 7.80 × 10^3 kg/m^3 and Poisson's ratio γ = 0.32.

Two kinds of cases are considered, including the air–blast of explosive without fragments and the arrangement of prefabricated fragments at the head of columnar explosive. The initial size of fragment is 36 mm × 36 mm × 2 mm, and fragments are contacted with and attached to grain. In order to study the influence law of fragment size on the attenuation of shock wave propagation, the prefabricated fragments at both ends are divided equally into 4, 9, 16, 25, 36, and 81 respectively. The arrangement of prefabricated fragment is shown in Fig. 5. In each case, TNT explosive equivalent is m_e = 400 g and the total mass of fragments at one end is 20.22 g, which are kept constant. Table 3 shows the specific calculation conditions of the changing fragment sizes.

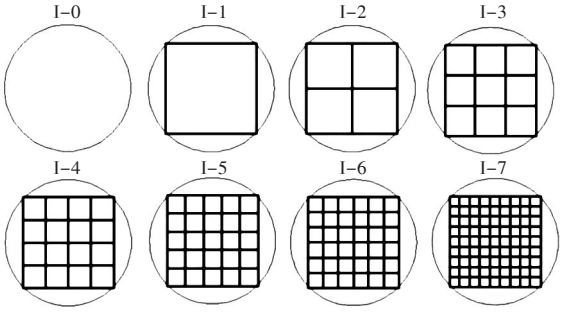

Fig.5 The arrangement of fragments

Table 3 Computational conditions

Number of cases	Side length of single fragment a /mm	Fragment thickness d /mm	Number of fragments at one end n
I–0	–	–	–
I–1	36	2	1
I–2	18	2	4
I–3	12	2	9
I–4	9	2	16
I–5	7.2	2	25
I–6	6	2	36
I–7	4	2	81

1.3 Validation of simulation method

In this paper, the air–blast shock waves test of cylindrical TNT explosive with the length–diameter ratio of 1.0–1.2 is simulated[17]. Fig. 6 shows the pressure contours of peak overpressure of shock wave at 7 m near the explosion, and the axial peak overpressure occurs near symmetry axis. Table 4 shows the comparison result of experimental averages and simulation values of peak overpressure of shock wave at four axial measuring points in the five tests. It can be seen from Table 4 that all errors are less than 20%, and numerical simulation results are closer to experimental averages, so simulation methods can be used in the next studies. Based on this simulation method, eight cases of I-0-I-7 are calculated, and the influence of fragment size on shock wave and fragment propagation is comparatively analyzed.

Fig.6 The contours of peak overpressure of shock wave at 7 m (t=11 376.7 μs)

Table 4 Comparison of the numerical and experimental results from Reference[17]

Distance/m	Data of peak overpressure		Error/%
	Experimental measurement/MPa	Numerical simulation/MPa	
3.5	0.257	0.271	5.45
5.0	0.124	0.135	8.87
7.0	0.099	0.094	–5.05
9.0	0.051	0.059	15.70

2 Simulation results and analysis

2.1 Influence of fragment size on the propagation and attenuation of air–blast shock wave

As can be found from the numerical simulation results of cases I-1–I-7, no matter whether it is a single large–mass fragment or small–mass fragment group which is placed intensively, the propagation waveforms from 0–200 μs are approximately the same. As shown in Fig. 7–Fig. 9, in the first stage of shock wave propagation, fragments hinder the propagation of shock wave right behind them, and waves on both sides flow around the fragments. Conical precursor wave is formed in the front of fragments due to high fragment velocity. The waves on both sides propagate in front of fragments, whose initial velocity is large. The second stage is at about 200 μs, where fragments catch up and exceed the shock waves that flow around. In the third stage, since the velocity of fragments is greater than that of the shock wave, fragments have been kept moving in in front of shock wave after exceeding it. However, through the analysis of Fig. 7–Fig. 9, it can be seen that shock wave lo-

cated right behind the fragments is obstructed by the fragments in the initial stage of propagation. It does not propagate in front of the fragments, and this is not obvious in the first stage of propagation. This is due to the chemical reaction occurring in explosion. The heat released quickly heats the detonation product and diffuses outwards at a high velocity, and the rapid propagation of detonation product make the air pressure, density and temperature increase suddenly, thus forming the initial shock wave. When prefabricated fragments are arranged at ends, the detonation products at the end of fragments act on fragments first, and a considerable part of the energy will be converted to the kinetic energy of fragments. In the early stage of explosion, shock wave velocity on both sides is greater than that of fragment, and it

(a) t=100 μs

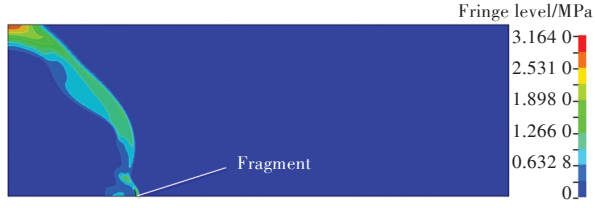

(b) t=200 μs

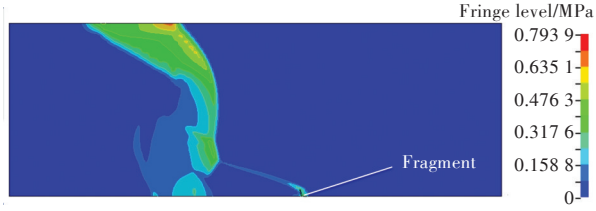

(c) t=500 μs

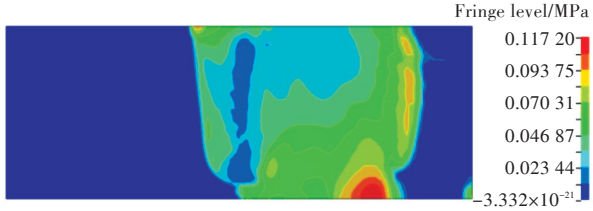

(d) t=2 000 μs

Fig.7 Pressure contours of the cases I-1

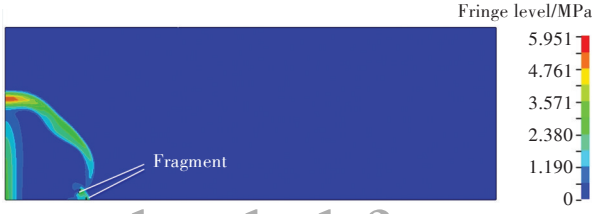

(a) t=100 μs

(b) t=200 μs

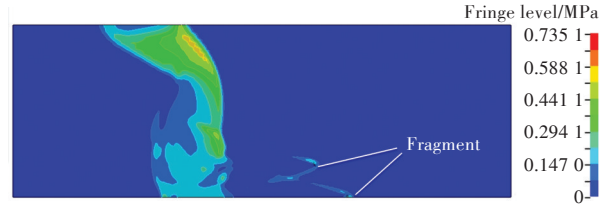

(c) t=500 μs

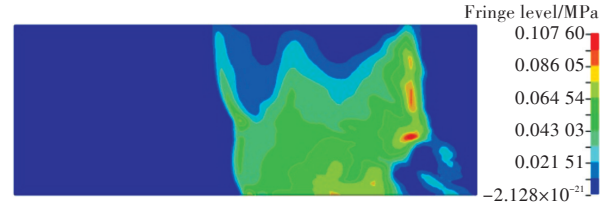

(d) t=2 000 μs

Fig.8 Pressure contours of the cases I-3

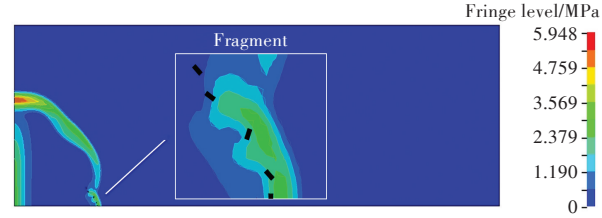

(a) t=100 μs

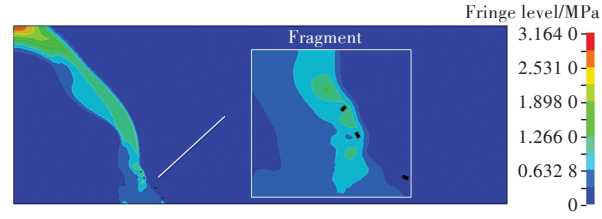

(b) t=200 μs

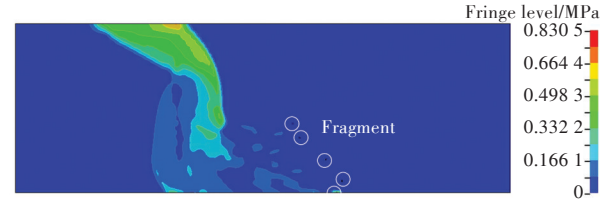

(c) t=500 μs

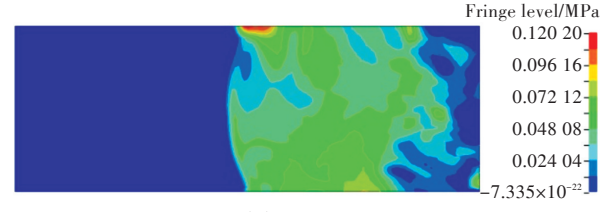

(d) t=2 000 μs

Fig.9 Pressure contours of the cases I-7

flows around to the front of the shock wave. In the propagation of fragments, the air in front of fragments is also compressed, forming precursor wave. Therefore, in the early stage of propagation of fragments and shock waves, the shock waves having flown around the fragments should propagate in front of the fragments in the previous stage.

As shown in the pressure contours at 2 000 μs moment in Fig. 7–Fig. 9, the pressure of peak shock wave is instable after being disturbed by fragments. The average overpressure of each unit of shock wave in the positive pressure space along one propagation direction at some moment is selected as the average overpressure of shock wave. The intensity of the shock wave in this direction is measured. At 2 000 μs, the average overpressure of shock wave containing prefabricated fragment in the direction of the explosive axis is about 0.06 MPa. While in the case of explosive air–blast without fragments, the average overpressure value of shock wave when it reaches the corresponding position is about 0.86 MPa. In the case of explosive air–blast without fragments, shock wave needs about 340 μs to pass through the measuring point at 0.7 m near the center of the explosion. Accordingly, in the case containing prefabricated fragments, the time that shock wave needs to pass through the measuring point at 0.7 m is 4–5 times as the one in the former case (Table 5). Therefore, it can be obtained that the presence of fragment group impedes the propagation of shock waves, which will greatly reduce the propagation velocity of shock wave.

Table 5 Average pressure of the blast wave in axial direction

Case	Time / μs	Average overpressure /MPa	Time that shock wave needs to pass through the measuring point at 0.7 m near the explosion center/μs
I–0	340	0.857 7	340
I–1	2 000	0.065 0	1 520
I–2	2 000	0.047 0	1 840
I–3	2 000	0.057 5	1 510
I–4	2 000	0.057 2	1 710
I–5	2 000	0.065 2	1 610
I–6	2 000	0.051 7	1 650
I–7	2 000	0.061 5	1 550

Fig. 10–Fig. 12 respectively show the peak pressure curve of shock waves at 0.3 m, 0.4 m and 0.5 m near the explosion center in the cases I-0, I-1, I-3, I-7. Fig. 13 shows the impulse value distribution of average ratio of shock wave in the mesh refinement area of models in each case at 0.3 m near the explosion center. Analysis of Fig. 10–Fig. 13 shows that fragment has a significant attenuation effect on shock wave. After taking the overpressure curve at 0.3 m (Fig. 10) as an example, we can see that in the case of explosive air–blast without fragments, the peak overpressure of the measuring point at 0.3 m is 7.94 MPa; the action time of overpressure peak is 70.5 μs; and the action time of positive pressure is 30.5 μs. While in the same measuring point, the peak overpressures of cases I-1, I-3, I-7 are respectively 2.12, 1.33 and 2.17 MPa; the action moments of peak overpressure are respectively 146.37, 131.9 and 126.7 μs; and the action time of positive pressure is respectively 116.5, 101.2 and 84.6 μs. This shows that peak overpressure of the case with prefabricated fragment is obviously lower than that of shock wave in the case of explosive air–blast of without fragments. The existence of prefabricated fragments postpones the action moment of peak shock wave, and increases the action time of positive pressure. The highest point of peak pressure curve in cases I-1, I-3 and I-7 is precursor wave of fragments, and the action moment of precursor wave is consistent with fragment propagation. By comparison, it can be seen that the existence of fragment group will reduce the peak overpressure of shock wave in the direction of fragment motion to a great extent, while greatly increases the action time of positive pressure. By analyzing the specific impulse scatter plot (Fig. 13), it can be seen that arranging prefabricated fragments at one end of the explosive and changing fragment sizes have small effects on the average ratio impulse near explosive axis. This indicates that the existence of fragment group can change the form of shock wave loads, but can hardly change the effect energy of shock wave.

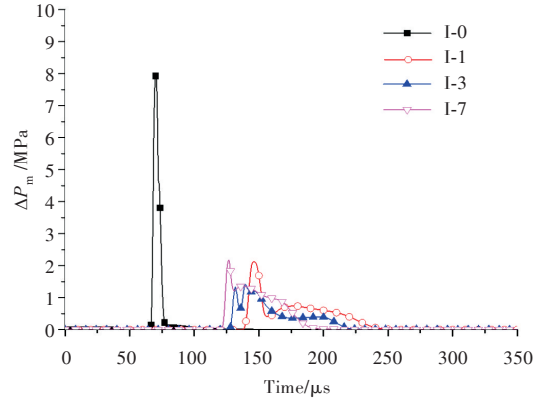

Fig.10 Peak overpressure of blast wave at 0.3 m

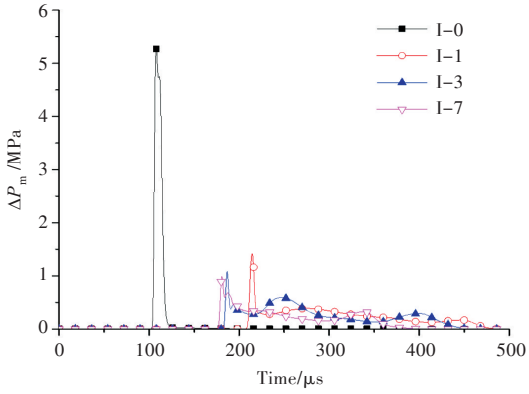

Fig.11 Peak overpressure of blast wave at 0.4 m

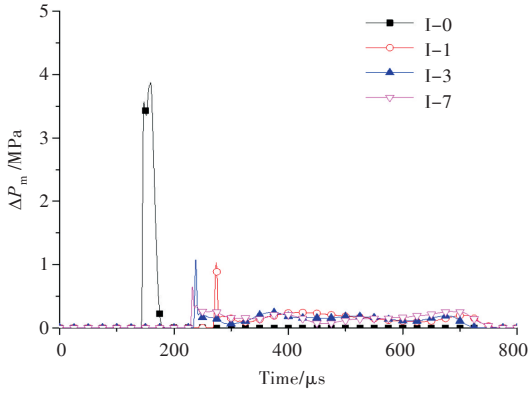

Fig.12 Peak overpressure of blast wave at 0.5 m

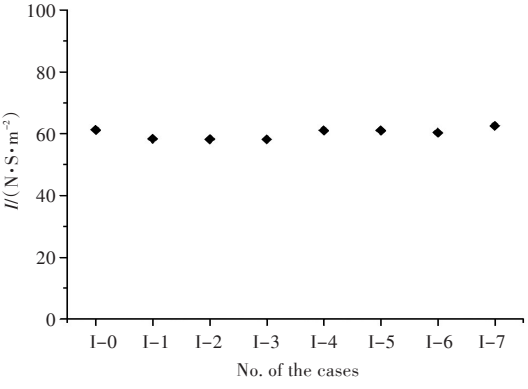

Fig.13 Data of specific impulse at 0.3 m

2.2 Influence of fragment size on the propagation and attenuation of fragment itself

The velocity and scattering angle of fragments are the important indicators to measure the killing power of warhead. Similar to the situation of detonation-driven plate[9], for the calculation case of attachment of cylindrical charge with prefabricated fragment to the end in this paper, it is assumed that the initial velocity of fragment group equals the casting velocity driving the overall plate movement, the scattering angle of discrete fragment linearly increases outwards from the center of explosion.

The computational model can be approximated as a single TNT explosion case with a plate with similar area attached to one end. The initiation method of one end detonation is adopted and explosive height H = 6.5 cm, radius R = 2.5 cm, density ρ_M = 1 590 kg/m^3, fragment thickness h_1 = 0.2 cm, and density ρ_1 = 7 800 kg/m^3. From the Gurney plate casting formula in Reference [9], the plate casting velocity of columnar TNT V_0=1 791.707 m/s can be obtained. Through simulation calculation, the average initial velocities of fragment group in cases I-1-I-7 are respectively V= 1 639.11, 1 631.08, 1 645.29, 1 673.21, 1 690.35, 1 693.52 and 1 721.71 m/s. All of them are smaller than the approximate calculation value of plate. However, from the perspective of relative error, the deviation is kept between 3.91%-8.97%, and the error is within the allowable range of engineering applications.

Fig. 14 shows the acceleration and attenuation of fragments before 760 μs. From Fig. 14, it can be seen that the variation of average initial velocity of fragments under different cases, the remaining average velocity at 760 μs and attenuation. It can be found from Fig. 14 and Fig. 15 that due to the acceleration of detonation products and shock wave, fragment can be accelerated to the highest velocity in a very short period of time. Afterwards, it shows a nearly linear attenuation, and there is no obvious fluctua-

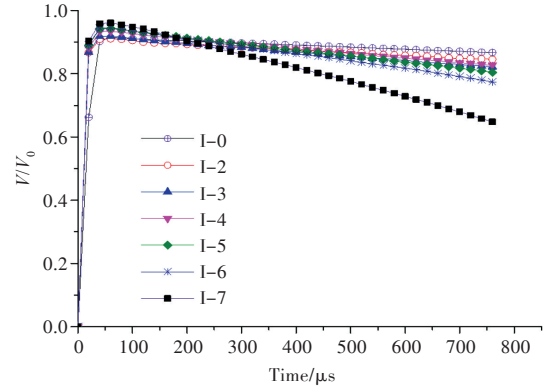

Fig.14 Velocity of the fragments

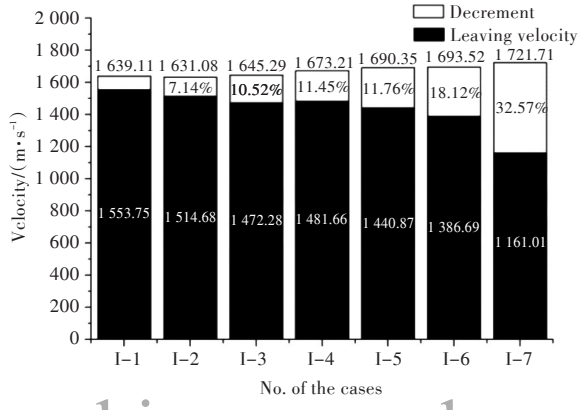

Fig.15 Decrement of velocity of the fragments

tion in the attenuation. The smaller the size of single fragment is, the higher the initial energy obtained by the fragment group is, resulting in a faster attenuation. At 760 μs, the velocity attenuation of fragment in cases I-1–I-7 is respectively 5.21% , 7.14% , 10.52%, 11.45%, 14.76%, 18.12% and 32.57%.

From Fig. 15, it can be further obtained that the smaller the fragment size of fragment group is, the greater the initial total kinetic energy obtained by the fragment group is. This is because the average velocity measured in this paper is the average velocity of the fragments in all directions. As shown in Fig. 16, for fragments with large mass, a portion of the energy in the early stage of explosion is transformed into the deformation energy of the fragments. While fragments with small mass are separated from each other, and are scattering in the radial and axial directions after being affected by the initial shock wave energy. The deformation degree of fragment is low, and more energy is converted into the kinetic energy of fragments.

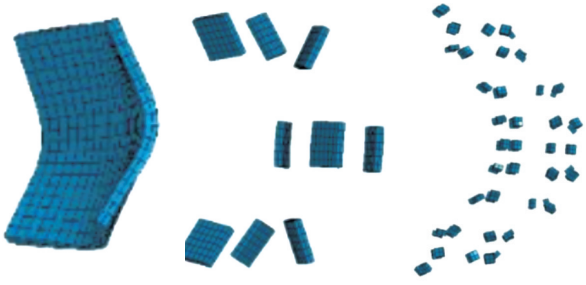

(a) I-1 (b) I-3 (c) I-7

Fig.16 The distribution of the fragments (t = 100 μs)

The attenuation laws of prefabricated fragments can be analyzed from two aspects:

1) Analyzing from the role of shock wave loads, it can be seen that the effect of shock wave on single fragment with large mass is basically equal to that on the fragment group with small mass which is intensively arranged in the early stage of explosion. However, small fragments spread with the propagation, and shock wave passes through the fragment gap, which reduces the intensity and duration of the continued effect of shock wave on fragments. In contrast, fragments with large mass can be continuously propelled by shock waves, and continue to obtain the energy transmitted by shock wave.

2) By analyzing the attenuation causes of fragment itself, it can be seen that although discrete fragments with small mass obtains high energy in the early stage and has faster initial velocity, the total windward area of it is larger. Therefore, it is subjected to larger resistance in the air, and velocity attenuates faster.

3 Conclusions

In this paper, finite element analysis software ANSYS/LS–DYNA is used to calculate explosive air–blast without fragments and the numerical simulation model in cases of 1, 4, 9, 16, 25, 36 and 81 prefabricated fragments with the total mass of 20.22 g, so as to study the attenuation laws of shock wave and fragments in the case with prefabricated fragments. The main conclusions are as follows:

1) The existence of prefabricated fragments will significantly weaken the intensity and velocity of the shock wave and obstruct the propagation of the shock wave right behind the fragment. Moreover, it can postpone the action moment of the shock wave, and increase the action time of positive pressure of shock wave.

2) If the total mass of fragments is kept unchanged, changing the size of a single fragment has little impact on the propagation of shock wave.

3) In the case of prefabricated fragments, the average initial velocity obtained by fragment group is close to the casting velocity of Gurney plate of a single columnar TNT explosive.

4) If the total mass and thickness of fragment group are kept unchanged, the smaller the size of a single fragment in fragment group is, the higher the initial total kinetic energy obtained by the fragment group is, but velocity attenuates faster.

References

[1] HOU H L, ZHU X, MEI Z Y. Study on the blast load and failure mode of ship structuresubject to internal explosion[J]. Explosion and Shock Waves, 2007, 27(2): 151–158 (in Chinese).

[2] LI M, ZHU X, HOU H L, et al. Numerical simulation of steel plates subjected to the impact of both impact waves and fragments[J]. Chinese Journal of Ship Research, 2015, 10(6): 60–67 (in Chinese).

[3] HUTCHINSON M D. The escape of blast from fragmenting munitions casings[J]. International Journal of Impact Engineering, 2009, 36(2): 185–192.

[4] YANG Y D, LI X D, BO X F. Influence of initiation mode on power of deformable directional warhead[J]. Journal of Nanjing University of Science and Technology, 2012, 36(5): 762–766, 772 (in Chinese).

[5] KONG X S, WU W G, DU Z P, et al. Research on fragments characteristic of cylindrical warheadwhen detonated at different points[J]. Journal of Harbin Engineering University, 2013, 34(7): 855–861 (in Chinese).

[6] KONG X S, WU W G, DU Z P, et al. Research on fragments characteristic of cylindrical warhead [J]. Engineering Mechanics, 2014, 31(1): 243-249 (in Chinese).
[7] LV X C, XU J Y, BAI E L, et al. Analysis of coupling between shrapnel and blast shock wave[J]. Journal of PLA University of Science and Technology, 2007, 8(6): 640-644 (in Chinese).
[8] ZHANG Q, MIAO C Q, BAI C H, et al. The influence of shell on blast shock wave intensity [J]. Chinese Journal of Applied Mechanics, 2003, 20(3): 145-147 (in Chinese).
[9] SUN Y B. 爆炸作用与装药设计[M]. Beijing: National Defense Industry Press, 1987(in Chinese)
[10] FENG S S, CUI B G. An experimental investigation for the axial distribution of initial velocity of shells [J]. Acta Armamentarii, 1987, 4(4): 60-63 (in Chinese).
[11] ZHANG Q, MIAO C Q, LIN D C, et al. Relation of fragment with air shock wave intensity for explosion in a shell [J]. International Journal of Impact Engineering, 2003, 28(10): 1129-1141.
[12] CHEN Y H, BAI C H, LIU Y, et al. Experimental study and initial velocity calculation of particles dispersed by center explosive [J]. Acta Armamentarii, 2012, 33(5): 556-559 (in Chinese).
[13] LIANG W M, ZHANG X Z, LIANG S F, et al. Experimental research on motion law of fragment and shock wave under the condition of internal explosion [J]. Acta Armamentarii, 2009, 30 (Supp 2): 223-227 (in Chinese).
[14] WANG R C, ZHAO G Z. 弹丸终点效应[M]. Beijing: Beijing Institute of Technology Press, 1993 (in Chinese)
[15] GONG C A, CHEN Z G, YIN L K. Analysis of movement laws of fragment and shock wave from a blast fragmentation warhead [J]. Journal of Measurement Science and Instrumentation, 2015, 6(3): 218-222.
[16] ZHANG Y. 杀爆战斗部对武装直升机的毁伤研究[D]. Nanjing: Nanjing University of Science and Technology, 2013(in Chinese)
[17] HU Z Y, TANG D G. Numerical simulation of TNT explosion in air[J]. Blasting, 2014, 12(4): 41-45 (in Chinese).
[18] HU C M, HE H L, HU S S. A study on dynamic mechancial behaviors of 45 steel [J]. Explosion and Shock Waves, 2003, 23(2): 188-192 (in Chinese).
[19] TANG T G, LI Q Z, SUN X L, et al. Strain-rate effects of expanding fracture of 45 steel cylinder shells-driven by detonation [J]. Explosion and Shock Waves, 2006, 26(2): 129-133 (in Chinese).
[20] ZHANG Q, QIN B, SUN Q Y, et al. Influence of thickness of warhead shell upon explosive shock wave [J]. Journal of Ballistics, 2008, 20(2): 17-19, 23 (in Chinese).
[21] ZHANG W, XIAO X K, WEI G. Constitutive relation and fracture model of 7A04 aluminum alloy [J]. Explosion and Shock Waves, 2011, 31(1): 81-87 (in Chinese).
[22] BOVIK T, HOPPERSTAD O S, DEY S, et al. Strength and ductility of Weldox 460 E steel at high strain rates, elevated temperatures and various stress triaxialities [J]. Engineering Fracture Mechanics, 2005, 72(7): 1071-1087.

破片尺寸对空爆冲击波及破片传播过程的影响仿真分析

郑红伟, 陈长海, 侯海量, 朱锡, 李典
海军工程大学 舰船工程系, 湖北 武汉 430033

摘　要: [**目的**] 为探讨高速破片与空爆冲击波相互作用下冲击波与高速破片的传播规律以及速度和能量衰减机制, [**方法**] 采用ANSYS/LS-DYNA软件建立端部贴有预制破片的柱状TNT空爆仿真模型。在破片总质量相同的情况下, 改变单个预制破片尺寸, 研究破片群单个破片尺寸对冲击波及破片自身传播过程的影响。[**结果**] 结果表明, 预制破片群会阻碍破片正后方冲击波的传播, 较大程度地降低冲击波的强度和传播速度; 在破片群总质量相同的情况下, 单个破片尺寸对冲击波传播的影响差异不大; 破片群的单个破片尺寸越小, 破片群获得的初始总动能越高, 但破片速度衰减越快。[**结论**] 因此, 在空爆冲击波和高速破片联合作用的研究中, 应主要考虑爆炸产生的破片尺寸差异对高速破片载荷的影响。这一结论可为战斗部空爆载荷特性及载荷联合作用研究提供参考。

关键词: 爆炸力学; 空爆冲击波; 高速破片; 数值仿真; 破片尺寸